

Hans Peter Ledermann, MD
William B. Morrison, MD
Mark E. Schweitzer, MD

Index terms:

Arthritis, septic, 46.26, 46.79
Bones, infection, 465.211, 466.211,
467.211
Cellulitis, 468.241
Foot, infection, 468.21, 468.241
Foot, MR, 468.121411, 468.121412,
468.121413, 468.121415
Soft tissues, infection, 468.241

Published online before print
10.1148/radiol.2233011279
Radiology 2002; 223:747–755

Abbreviations:

SE = spin echo
STIR = short inversion time
inversion-recovery

¹ From the Department of Radiology, Thomas Jefferson University Hospital, Philadelphia, Pa. Received July 26, 2001; revision requested September 12; revision received October 30; accepted December 10. **Address correspondence** to H.P.L., Department of Radiology, University Hospital Basel, Petersgraben 4, 4031 Basel, Switzerland (e-mail: hans-peter.ledermann@gmx.ch).

© RSNA, 2002

Author contributions:

Guarantors of integrity of entire study, H.P.L., M.E.S.; study concepts, W.B.M., M.E.S.; study design, H.P.L., W.B.M.; literature research, H.P.L.; clinical studies, H.P.L., W.B.M., M.E.S.; data acquisition, H.P.L.; data analysis/interpretation, H.P.L., W.B.M.; statistical analysis, H.P.L.; manuscript preparation and definition of intellectual content, H.P.L., W.B.M., M.E.S.; manuscript editing, H.P.L.; manuscript revision/review and final version approval, W.B.M., M.E.S.

MR Image Analysis of Pedal Osteomyelitis: Distribution, Patterns of Spread, and Frequency of Associated Ulceration and Septic Arthritis¹

PURPOSE: To evaluate the anatomic distribution of pedal osteomyelitis and septic arthritis in a large patient group with advanced pedal infection and to compare ulcer location with the distribution of osteomyelitis and septic arthritis.

MATERIALS AND METHODS: Contrast material-enhanced magnetic resonance (MR) imaging findings were reviewed for 161 feet in 51 women and 107 men (82% of whom had diabetes mellitus) who were suspected of having osteomyelitis and who underwent tissue diagnosis. Location of skin ulceration and presence of osteomyelitis (indicated by means of low T1-weighted signal intensity, high T2-weighted signal intensity, and contrast enhancement) and septic arthritis (indicated by synovial enhancement and adjacent cellulitis) were evaluated by two musculoskeletal radiologists.

RESULTS: In the forefoot, osteomyelitis occurred most frequently at the fifth metatarsal ($n = 24$), first metatarsal ($n = 21$), and first distal phalanx ($n = 15$). In the hindfoot, the calcaneus ($n = 21$) was involved most frequently. Osteomyelitis was directly adjacent to skin ulcers or surgical defects in all cases but one. Spread of osteomyelitis to adjacent bones in the forefoot occurred in 26 (16%) bones. Evidence of septic arthritis on MR images was present in 53 (33%) feet and involved most frequently the fifth ($n = 13$) and first ($n = 8$) metatarsophalangeal joints.

CONCLUSION: Pedal osteomyelitis results almost exclusively from contiguous infections and occurs most frequently around the fifth and first metatarsophalangeal joints. One-third of patients with advanced pedal infection show evidence of septic arthritis on MR images.

Foot ulcers and associated complications are a major source of morbidity and use of medical resources in patients with diabetes mellitus (1,2). Although many ulcers are superficial and heal with conservative treatment, up to 15% of patients with diabetes will develop a chronic nonhealing ulcer during their lifetime (3). In a study that included 8,905 diabetic patients, 514 (6%) developed a foot ulcer during a 3-year period of observation, and 77 (15%) of the 514 developed osteomyelitis (4). It was estimated that osteomyelitis complicates up to one-third of diabetic foot infections that require hospitalization (5). Septic arthritis is also a common complication of deep infection (6), since many pedal ulcers are located near joints.

Recently, magnetic resonance (MR) imaging has been increasingly used to evaluate the extent of pedal infections and to diagnose underlying osteomyelitis. Furthermore, MR imaging allows assessment of the presence and location of pedal ulcers (7) and the presence of concomitant septic arthritis (8,9).

This study was undertaken to evaluate the anatomic distribution of pedal osteomyelitis and septic arthritis in a large patient group with advanced pedal infection and to compare ulcer location with the distribution of osteomyelitis and septic arthritis.

MATERIALS AND METHODS

Patients

MR imaging findings of 161 feet in 158 patients (51 women, 107 men; mean age, 58.5 years; age range, 20–99 years) were reviewed. This group included all patients from our institution between July 1995 and March 2000 who underwent pedal MR imaging and tissue diagnosis (including bone culture and/or histopathologic evaluation) after MR imaging to evaluate the presence of osteomyelitis. The clinical history of these patients included diabetes mellitus ($n = 130$), paraplegia ($n = 5$), prior trauma ($n = 6$), vascular disease ($n = 4$), bad hygiene due to mental disorder ($n = 3$), intravenous drug abuse ($n = 2$), and other entities ($n = 8$) such as sickle cell disease, postoperative deformity, multiple sclerosis, ingrown toenails, alcohol abuse, frostbite, vascular embolism, and enchondroma.

One or more surgical procedures were performed on 49 feet prior to MR imaging. These included débridement ($n = 24$), toe amputation ($n = 13$), ray amputation ($n = 9$), transmetatarsal amputation ($n = 4$), internal reduction of a fracture ($n = 3$), and Chopart amputation ($n = 1$). The interval between these surgical procedures and MR imaging ranged between 2 days and 6 years (mean, 235 days \pm 440 [SD]).

Our study was conducted after approval was obtained from our institutional review board to review patient images and medical charts. The board determined that this retrospective study could be conducted without informed patient consent.

MR Imaging

MR imaging was performed with a 1.5-T superconducting magnet (Signa; GE Medical Systems, Milwaukee, Wis). An extremity coil was used to image a total of 155 feet (field of view, 14–20 cm), and a head coil was used with six patients who underwent imaging of both feet (field of view, 16–20 cm). In the patients who underwent simultaneous imaging of both feet, subsequent surgery or biopsy was performed in only one foot per patient, and only that foot was included in the study. Images of all feet were obtained by means of at least two orthogonal planes.

T1-weighted spin-echo (SE) images were obtained with one to two signals acquired, a repetition time of 400–750 msec and an echo time of 8–20 msec (400–750/8–20), and a matrix size of 256×192 or $256 \times$

256. T2-weighted images were obtained by using a fast SE technique with two signals acquired, 2,000–7,800/75–108 (effective), an echo train length of eight, and a matrix size of 256×128 or 256×192 . Contrast material-enhanced T1-weighted images were obtained in 30 feet by using a T1-weighted SE sequence and in 131 feet by using a fast multiplanar spoiled gradient-echo technique with 200–305/1.8–2.2, a flip angle of 90° , and a matrix size of 256×128 or 256×192 . Gadopentetate dimeglumine (Magnevist; Berlex Laboratories, Wayne, NJ) at a dose of 0.1 mmol per kilogram of body weight was used as the intravenous contrast agent. T1-weighted fast multiplanar spoiled gradient-echo sequences were performed with fat suppression before and after contrast agent administration. For T2-weighted and gadolinium-enhanced T1-weighted SE sequences, fat suppression was accomplished by using selective presaturation of lipid-resonance frequency. Fast SE short inversion time inversion-recovery (STIR) images were obtained with an echo train length of eight, 2,000–3,000/20–78 (effective), an inversion time of 150–160 msec, and a matrix size of 256×128 or 256×192 . Fast SE STIR images were available for a total of 137 feet. Section thickness was 4 mm, and there was a 1-mm gap for most sequences.

Image Analysis

Diagnosis of a skin ulcer relied on recognition of a soft-tissue defect or an interruption of the skin line on any imaging sequence or plane (7). Cellulitis was defined as soft-tissue contrast enhancement with fat signal loss on T1-weighted images and hyperintense signal intensity on T2-weighted images when compared with that of surrounding muscle, as described by prior authors (9,10).

MR imaging criteria for the diagnosis of osteomyelitis were based on those described in previous studies (8,11), including focally decreased marrow signal intensity on T1-weighted images, focally increased signal intensity on fat-suppressed T2-weighted and fast SE STIR images, and focal marrow enhancement on gadolinium-enhanced fat-suppressed T1-weighted images. Osteomyelitis was also diagnosed if focal decrease of marrow signal intensity was absent on T1-weighted images in the presence of signal intensity increase on T2-weighted images and contrast-enhanced images (ie, discordant marrow signal intensity), as previously reported (7,12). Osteomyelitis in contiguous bones without evidence of direct infection of both bones by an ulcer or surgical defect was defined

as osseous spread of osteomyelitis. The bone that had direct contact with the ulcer was defined as the primary bone. Evidence of septic arthritis had to be present between bones on MR images to qualify as osseous spread.

MR imaging criteria for the presence of septic arthritis were contrast enhancement of the joint capsule (10) and adjacent soft-tissue infection (13,14). Increased joint fluid was not necessary for this diagnosis, since erosion of the joint capsule of digital joints can lead to decompression of joint effusion.

To facilitate data acquisition, a spreadsheet was designed that contained two schematic drawings of the bones of the foot and ankle with anteroposterior and lateral projections. The foot and ankle were divided into three anatomic regions: forefoot (from the toes to the Lisfranc joint), midfoot (from the Lisfranc joint to the Chopart joint), and hindfoot (from the Chopart joint to the ankle joint, including the malleoli).

Two musculoskeletal radiologists (W.B.M., M.E.S.) reviewed all images by means of consensus. The reviewers were blinded to patient history and the presence and location of an ulcer. They did, however, know that all images were obtained to evaluate the presence of osteomyelitis. First, the reviewers determined the location of the ulcer or surgical defect on the MR images and noted its position in the anatomic diagram on the spreadsheet. Skin ulcerations and soft-tissue defects at postoperative sites of amputations and débridements were analyzed separately. Since postoperative soft-tissue defects often extended over an area of several bones, we noted the presence of such defects for each underlying bone separately.

Next, the reviewers determined the presence and location of osteomyelitis and septic arthritis on the MR images and marked their positions on the spreadsheet. In cases of contiguous spread of osteomyelitis from one bone to another, all infected bones and the direction of spread (ie, proximal or distal) were noted.

Comparison with Reference Standards

After MR imaging, percutaneous or surgical biopsy was performed to evaluate the presence of osteomyelitis. The date and nature of surgical interventions performed on the feet prior to MR imaging were reviewed, and the date and type of surgical treatment performed after MR imaging were recorded. Charts and surgical reports were reviewed for all patients

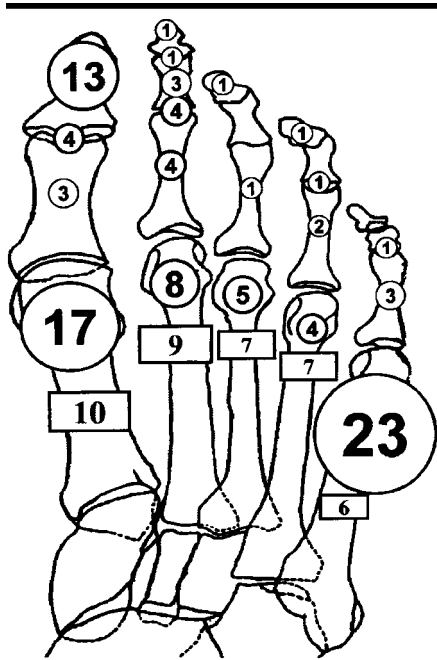


Figure 1. Synopsis of the anatomic distribution of ulcers in all 161 feet in which MR imaging was performed (the total number of observed ulcers per location is provided in circles). The distribution of ulcers or skin defects at postoperative sites is summarized separately for each involved metatarsal bone (in rectangular boxes).

by the author (H.P.L.) who was not involved in image interpretation.

The following procedures were performed after MR imaging: toe amputation ($n = 44$), débridement ($n = 37$), ray amputation ($n = 33$), amputation below the knee ($n = 16$), transmetatarsal amputation ($n = 16$), Chopart amputation ($n = 7$), percutaneous bone biopsy ($n = 5$), amputation above the knee ($n = 3$), and foot amputation ($n = 1$). To avoid both contamination of the bone biopsy samples by adjacent soft-tissue infection and inoculation of potentially sterile bone, percutaneous bone biopsy was performed in only a minority ($n = 5$) of patients. Care was taken to pass the 12-gauge needles through intact, uninfected soft tissue into the bone. All other bone biopsies were performed by the surgeons themselves during surgical procedures. Pathologic findings of bone samples were available for all patients, and microbiologic findings were available for 112 patients.

If the location of an ulcer or surgical defect was adequately described on a patient chart, then this location was compared with the location observed on MR images as determined by the two reviewers. Diagnosis of osteomyelitis with the use of MR imaging was verified in all patients

with review of microbiologic and pathologic reports. A positive diagnosis of osteomyelitis was established by means of culture growth or characteristic histologic findings of osteomyelitis. These histologic findings included aggregates of inflammatory cells (including neutrophils, lymphocytes, histiocytes, and plasma cells), erosions of trabecular bone, and marrow signal intensity changes that ranged from loss of normal marrow fat with acute osteomyelitis to fibrosis and reactive bone formation with chronic disease.

Diagnosis of septic arthritis was verified with review of surgical reports. The presence of associated conditions, such as diabetes mellitus, peripheral vascular disease, and postoperative or posttraumatic sequelae, were noted.

Data Analysis

We compared the histologic and culture findings of bone samples with MR imaging findings and calculated sensitivity and specificity values for the use of MR imaging in the diagnosis of osteomyelitis. After comparing the presence and location of skin ulcers as described in patient charts and surgical reports with that determined at MR image analysis, we calculated the sensitivity of MR imaging in the diagnosis of skin ulcerations.

RESULTS

In the 130 examinations of forefoot infections, 120 sites of skin breakdown were found on MR images (Fig 1). The three locations that were most frequently involved were the skin adjacent to the fifth metatarsal ($n = 23$, 19%), the first metatarsal ($n = 17$, 14%), and the distal phalanx of the first toe ($n = 13$, 11%). The toes with the most ulcers were the first ($n = 20$, 17%) and second ($n = 13$, 11%). Eleven of the 43 (26%) toe ulcers were situated dorsally ($n = 9$) or medially ($n = 2$) (Fig 2). Of these 11 ulcers, four were located over the interphalangeal joint of the first toe, and four were located at the proximal interphalangeal joint of the second toe. Three of the 11 ulcers were situated on the dorsal aspect of the proximal phalanx of the third, fourth, and fifth toes. The first ($n = 37$) and fifth ($n = 27$) rays had the most ulcers. The second ray had 21 ulcers, the fourth ray had eight ulcers, and the third ray had seven ulcers.

Additionally, there were 10 ulcerations at sites of previous amputations and 10 postoperative soft-tissue defects (Fig 3) around the distal metatarsal bones. The preceding interventions at these 20 sites

included ray amputations ($n = 8$), transmetatarsal amputations ($n = 4$), débridements ($n = 5$), and toe amputations ($n = 3$). Twelve of these sites had soft-tissue defects near several adjacent metatarsal bones. The resulting ulcers and soft-tissue defects at all 20 postoperative sites are summarized separately for each involved metatarsal bone in Figure 1.

There was proven osteomyelitis in 95 of 130 (73%) forefoot infections. The distribution of osteomyelitis in the forefoot mirrored the pattern of skin ulceration (Fig 4): The most frequently infected bones were the fifth metatarsal ($n = 24$), the first metatarsal ($n = 21$), and the distal phalanx of the first toe ($n = 15$). The toes most involved with osteomyelitis were the first ($n = 28$) and second ($n = 22$). Most bone infections were seen in the first ($n = 49$) and fifth ($n = 38$) rays. The third ray was the least involved, with 16 infected bones. Frequency of osteomyelitis decreased in rays 2–5 from proximally to distally. In the first toe, infection involved the distal phalanx more often than the proximal phalanx.

All MR images that demonstrated osteomyelitis of the forefoot showed contiguous spread of infection from a skin ulcer or postoperative skin defect. One hundred thirty-six of the 162 (84%) infected bones in the forefoot were near a skin ulcer or postoperative skin defect. In 26 (16%) bones, there was evidence of osseous spread from one bone to the other, with septic arthritis of the joint between them. Osseous spread was directed distally in 20 (77%) bones and proximally in six (23%) bones. Distally directed spread from the metatarsal heads to the proximal phalanges occurred in 17 feet, involving the fifth ($n = 9$), first ($n = 4$), second ($n = 3$), and fourth ($n = 1$) rays. Further distal spread of osteomyelitis was seen in the first ($n = 2$) and second ($n = 1$) toes and spread to the distal phalanx and middle phalanx, respectively. Proximal osseous spread was seen in six feet and spread to the proximal phalanx of the first, second, and fourth toes; to the middle phalanx of the fourth toe; and to metatarsal heads two and four.

Evidence of septic arthritis was seen in 53 (33%) feet and involved most frequently the fifth ($n = 13$) and first ($n = 8$) metatarsophalangeal joints in the forefoot (Fig 5), which was similar to the distribution of ulcers and osteomyelitis. The most frequently affected rays were the second ($n = 16$), first ($n = 14$), and fifth ($n = 14$).

The only patient who had a midfoot ulceration was a patient with neuropathic osteoarthropathy and a rocker-bottom deformity of the foot with osteo-

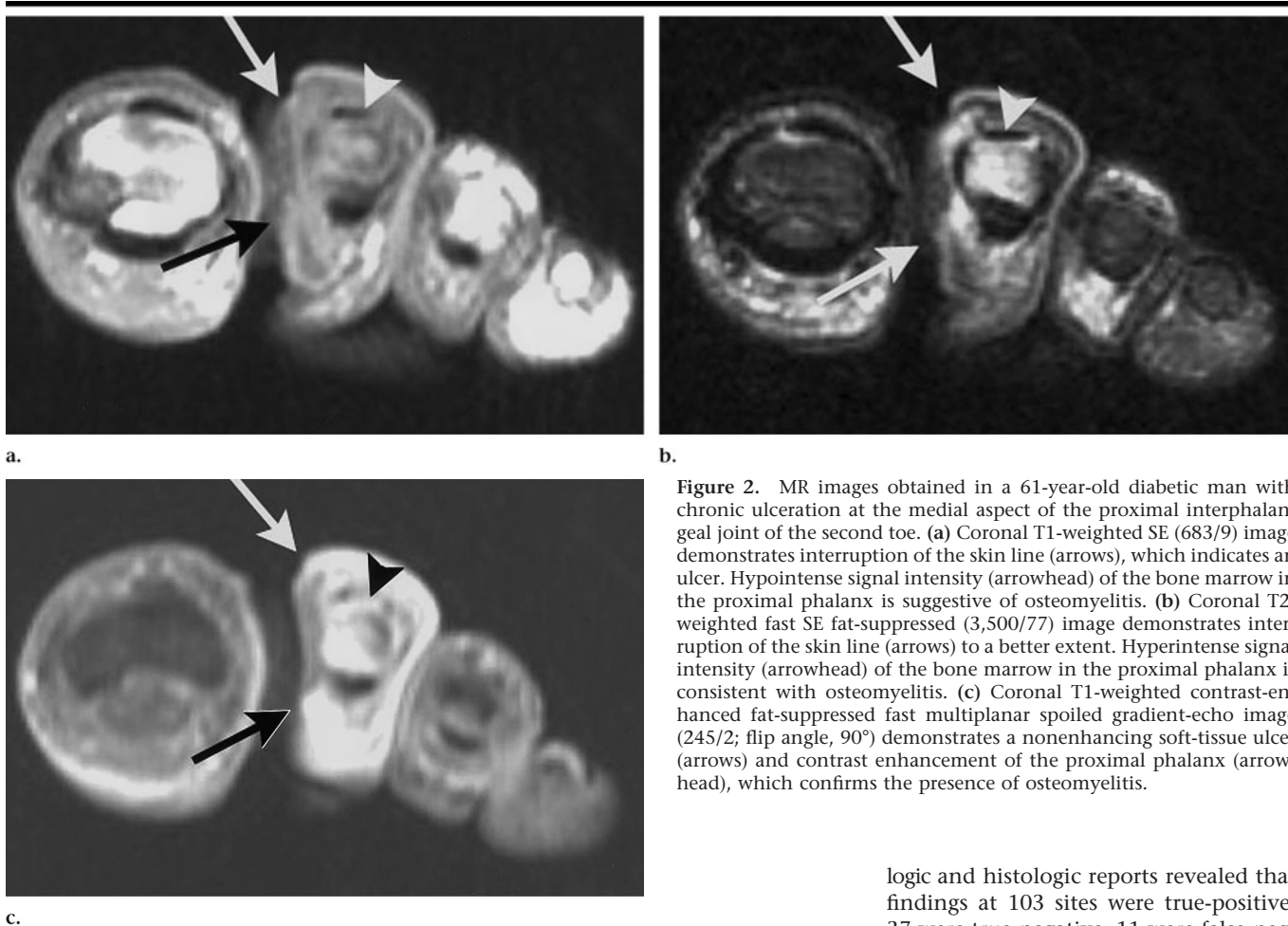


Figure 2. MR images obtained in a 61-year-old diabetic man with chronic ulceration at the medial aspect of the proximal interphalangeal joint of the second toe. (a) Coronal T1-weighted SE (683/9) image demonstrates interruption of the skin line (arrows), which indicates an ulcer. Hypointense signal intensity (arrowhead) of the bone marrow in the proximal phalanx is suggestive of osteomyelitis. (b) Coronal T2-weighted fast SE fat-suppressed (3,500/77) image demonstrates interruption of the skin line (arrows) to a better extent. Hyperintense signal intensity (arrowhead) of the bone marrow in the proximal phalanx is consistent with osteomyelitis. (c) Coronal T1-weighted contrast-enhanced fat-suppressed fast multiplanar spoiled gradient-echo image (245/2; flip angle, 90°) demonstrates a nonenhancing soft-tissue ulcer (arrows) and contrast enhancement of the proximal phalanx (arrowhead), which confirms the presence of osteomyelitis.

myelitis of the medial cuneiform bone, intermediate cuneiform bone, and second metatarsal base (Fig 6).

In 32 of all 161 (20%) MR examinations, there was evidence of hindfoot infection. All but one had evidence of skin ulceration on MR images. Most ulcers were seen at the heel ($n = 23$) and the lateral malleolus ($n = 4$). Two ulcers were seen over the medial malleolus, one was seen over the Achilles tendon, and one was seen over the dorsum of the hindfoot.

Twenty-four (75%) hindfoot infections had proven osteomyelitis that involved the calcaneus ($n = 21$) most frequently. Other infected bones were the lateral malleolus ($n = 5$), talus ($n = 4$), tibia ($n = 2$), and navicular bone ($n = 1$). One patient with a history of intravenous drug abuse and endocarditis had hematogenous osteomyelitis of the tibia and fibula (Fig 7). There was evidence of septic arthritis in five ankle joints and two subtalar joints.

Review of patient charts allowed accurate determination of the presence and location of an ulcer or surgical defect in 102

(63%) feet. In only three clinical examinations, however, did the report state that there was an absence of foot ulceration. Ninety-seven ulcers were identified correctly with MR imaging. Five ulcers were not recognized during MR image evaluation (sensitivity, 95%). Ulceration was correctly excluded in two of the three feet with documented lack of ulceration, but in one foot that had an irregular skin surface in the gangrenous forefoot region, ulceration was falsely diagnosed.

After MR imaging, all patients underwent either surgery or percutaneous bone biopsy, which included the following procedures: toe amputation ($n = 44$), débridement ($n = 37$), ray amputation ($n = 33$), amputation below the knee ($n = 16$), transmetatarsal amputation ($n = 16$), Chopart amputation ($n = 7$), percutaneous bone biopsy ($n = 5$), amputation above the knee ($n = 3$), and foot amputation ($n = 1$). The interval between MR imaging and surgery ranged between 1 and 66 days (mean, 9.3 days \pm 12.3). Comparison of MR imaging interpretations of osteomyelitis with patho-

logic and histologic reports revealed that findings at 103 sites were true-positive, 37 were true-negative, 11 were false-negative, and 10 were false-positive. This resulted in a sensitivity of 90.4% and a specificity of 78.7% for the diagnosis of osteomyelitis with the use of MR imaging. Discordant marrow signal intensity in infected bones with normal signal intensity on T1-weighted images and hyperintense signal intensity on T2-weighted and contrast-enhanced images (7,12) was seen in four feet in which MR imaging was performed in our study.

Presence of septic arthritis was confirmed with review of surgical reports for 17 feet and included the interphalangeal joint ($n = 1$), the metatarsophalangeal joint ($n = 14$), and the ankle joint ($n = 2$). In most of the other feet with evidence of septic arthritis on MR images, amputation was performed proximally without dissection of the infected joint.

DISCUSSION

Foot ulceration, a major cause of disability in patients with diabetes mellitus, results from a combination of causes. The triad of peripheral neuropathy, peripheral arterial disease, and susceptibility to

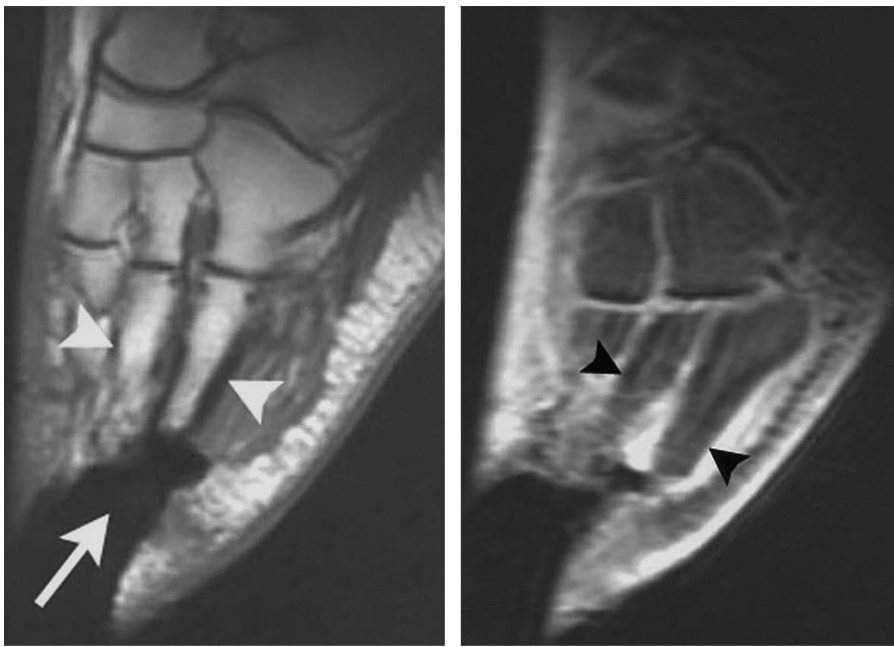


Figure 3. MR images obtained in a 57-year-old diabetic man who underwent partial ray resection of the fifth and fourth metatarsal heads 9 months prior to MR imaging and had a nonhealing wound. (a) Sagittal T1-weighted SE (500/8) image of the forefoot shows a large postoperative defect (arrow) at the lateral forefoot. Note normal marrow signal intensity of the fifth and fourth metatarsal bones (arrowheads). (b) Sagittal T1-weighted fat-suppressed contrast-enhanced fast multiplanar spoiled gradient-echo image (250/2.1; flip angle, 90°) confirms the absence of osteomyelitis with normal marrow signal intensity (arrowheads) at the stumps of the fifth and fourth metatarsal bones. Débridement of the fifth metatarsal bone was performed after MR imaging and proved the absence of osteomyelitis.

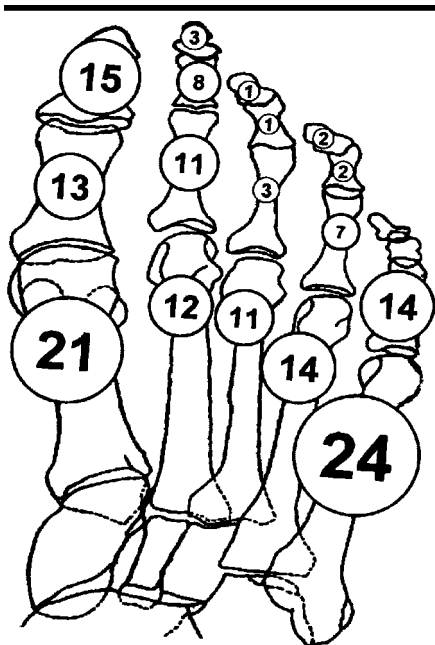


Figure 4. Summary of the anatomic distribution of osteomyelitis as observed on MR images. Numbers in circles indicate the sum of infected bones observed at that location.

infection are the primary predisposing risk factors for foot ulceration (15). The locations of ulceration correspond with the areas of highest pressure (16) during ambulation, and elevated plantar pressure has a high sensitivity for the prediction of ulceration in diabetic patients (17,18). The distribution of ulcers also depends on gait characteristics, type of footwear, and activity level, since all of these factors play important roles in the final accumulated mechanical trauma that the foot experiences (19). Similarly, the distribution of chronic deep foot infection may differ from the distribution of superficial ulcers in ambulatory patients, since the effectiveness of wound healing may vary with ulcer location (20).

All pedal infections but one in our patient population resulted from contiguous spread from an ulcer or skin defect. Most ulcers in our patient group that were clinically suggestive of osteomyelitis were seen around the fifth and first metatarsal heads and the distal phalanx of the great toe. Ulceration below the first metatarsophalangeal joint is commonly cited to be the most frequent location in the feet of

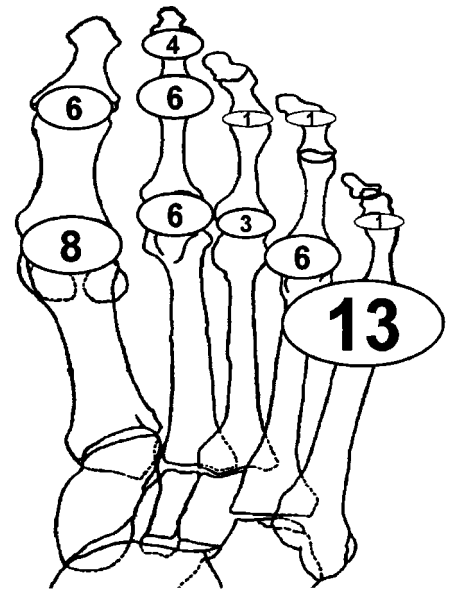


Figure 5. Anatomic distribution of septic arthritis as observed on MR images. Numbers in ovoids indicate the sum of observed septic joints at that location.

diabetic patients (21) and often results from deformity (eg, hallux valgus) and limited mobility of the first metatarsophalangeal joint (22,23). Ulceration around the fifth metatarsophalangeal joint was reported in only a minority of ambulatory patients (16), however, or was equal in frequency to the occurrence of ulcers below the second to fourth metatarsal heads in another study (23). Interestingly, most reports (1,24–27) provide only the total number of toe or metatarsal ulcers without providing the number of ulcers for each toe or metatarsal head. If ulceration of one ray is provided separately, then only the frequency of ulceration of the first ray is described (24,27).

Predominant involvement of the fifth metatarsal head in our study cannot be explained with a normal plantar foot pressure pattern, since normal biomechanical forces lead to high plantar pressures at the first and second metatarsal heads and the plantar aspect of the first toe (28). It has been shown, however, that foot deformities such as forefoot varus and valgus (29) or the presence of a rigid, plantar, flexed first ray (30) result in excessive plantar pressure around the fifth metatarsal head with subsequent ulceration. Predominant ulceration below the fifth metatarsal head in our study may therefore have been due to the selection of patients with such foot deformities. Alternatively, increased mechanical friction at the lateral border of the

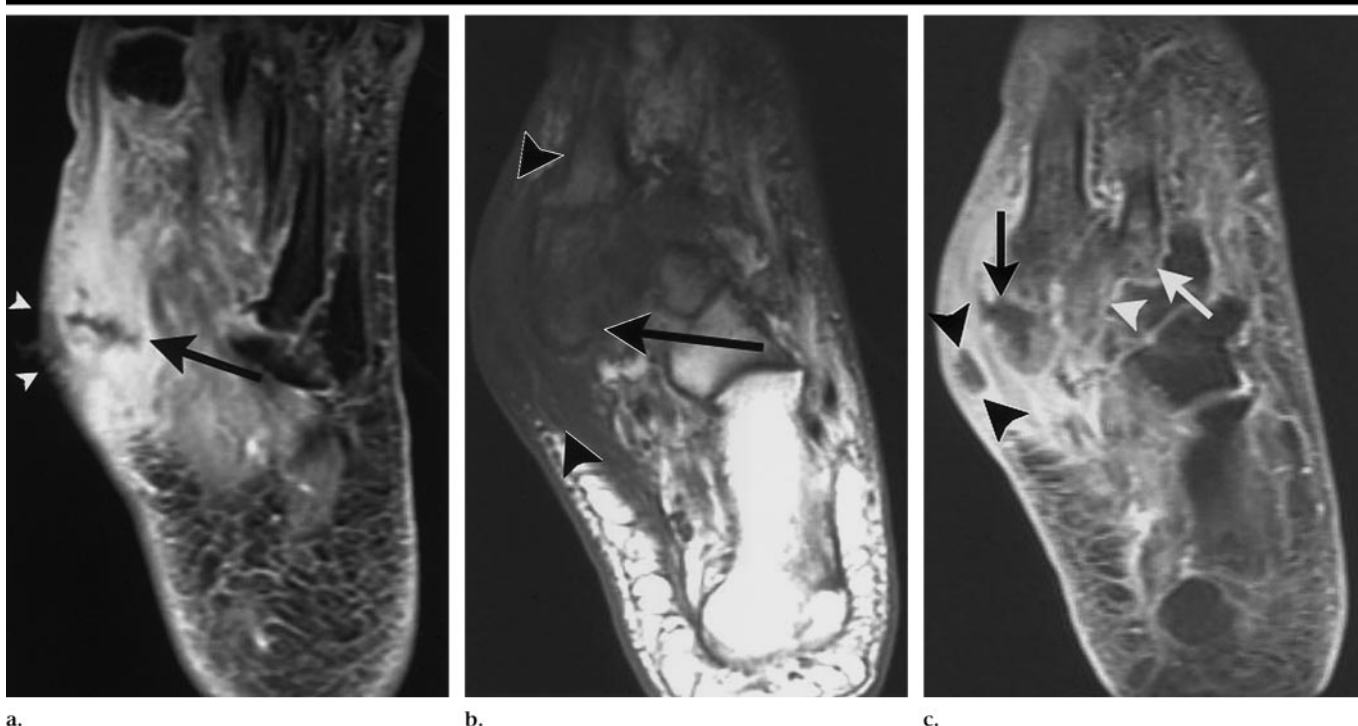


Figure 6. MR images obtained in a 52-year-old diabetic man with a rocker-bottom deformity of the midfoot as a result of Charcot arthropathy. (a) Transverse T1-weighted contrast-enhanced fat-suppressed fast multiplanar spoiled gradient-echo image (250/2.1; flip angle, 90°) demonstrates an ulcer (arrowheads) at the medial plantar aspect of the midfoot and a sinus tract (arrow) that extends into the medial plantar compartment. (b) Transverse T1-weighted SE (517/8) image obtained at a more dorsal level demonstrates extensive replacement of fat signal intensity in the subcutaneous tissue (arrowheads), which indicates cellulitis, and low signal intensity in the bone marrow of the first cuneiform bone (arrow), which indicates osteomyelitis. (c) Transverse T1-weighted contrast-enhanced fat-suppressed fast multiplanar spoiled gradient-echo image (305/2; flip angle, 90°) demonstrates a small, rim-enhancing, subcutaneous abscess (black arrowheads). Geographically demarcated hypointense signal intensity in the first cuneiform bone (black arrow) with surrounding contrast enhancement indicates intraosseous abscess formation. There is also osteomyelitis of the second cuneiform bone (white arrowhead) and osteomyelitis of the adjacent second metatarsal base (white arrow).

foot may impede healing of ulcers, with progression to deep infection.

One-fifth of toe ulcerations were observed dorsally, reflecting the frequent occurrence of claw-toe deformity in the feet of diabetic patients, with resulting friction against footwear and excessive pressure over the dorsal aspect of the toes (31). Clawing of the toes is thought to arise from motor neuropathy of the intrinsic muscles and may also lead to ulceration below the metatarsal heads because of anterior displacement of the fat pad from under the metatarsal heads (31). Only one of our patients had a mid-foot ulceration, and this was associated with a rocker-bottom deformity that resulted from Charcot arthropathy of the midfoot (29) (Fig 6).

We observed ulcerations at 10 amputation sites in the forefoot. It has been previously reported (32,33) that partial foot amputations interfere with normal biomechanics and may lead to focally increased plantar pressures with subsequent ulceration.

Bone infection was most frequently

present in our study at the fifth and first metatarsal bones and at the distal phalanx of the first toe. Since almost all bone infections in our study represented contiguous infections from skin ulcerations or postoperative defects, a close association between the locations of ulceration and osteomyelitis was observed. To the best of our knowledge, only one study (34) has provided the distribution of pedal osteomyelitis. The authors describe a similar distribution pattern of pedal osteomyelitis in their 42 diabetic patients to that in our patients, with decrease of frequency of osteomyelitis in rays 2–5 toward the distal phalanges and predominant involvement of the distal phalanx in ray 1. Osteomyelitis of the midfoot was also rare in that study, and the calcaneus was the most frequently infected bone in the hindfoot (34), as observed in our study group.

Septic arthritis is a well-known complication of advanced diabetic foot infection that occurs around the metatarsophalangeal and interphalangeal joints, but to our knowledge, its incidence has

not been analyzed or reported in the literature. In our patient group, one-third of all feet had evidence of septic arthritis on MR images. MR signal intensity characteristics indicative of septic arthritis, such as increased joint fluid and thickening of the synovium with contrast enhancement, are also seen in inflammatory arthropathies and are nonspecific (13,35). Graif et al (14) have reported that the combination of bone erosions and marrow edema is highly suggestive of a septic articulation. In pedal infections, the diagnosis of a septic joint with the use of MR imaging may be more specific, however, since ulceration and adjacent soft-tissue infection directly abut the joint. MR imaging often demonstrates sinus tracts that extend into the joint with obvious destruction of the joint capsule or the joint itself. Increased intraarticular fluid may not be evident in the small interphalangeal joints, especially if the joint capsule is eroded, and it is therefore not a valuable MR imaging criterion for septic arthritis. It has also been shown that even infections in larger joints, such



Figure 7. MR images obtained in a 24-year-old man with a history of intravenous drug abuse and acute ankle pain without evidence of ulceration or penetrating skin defect. (a) Sagittal T1-weighted SE (600/8) image of the hindfoot shows hypointense swelling (arrows) of the ankle joint, which is compatible with effusion and hypointense signal intensity of the bone marrow of the tibia. (b) Sagittal T1-weighted contrast-enhanced fat-suppressed fast multiplanar spoiled gradient-echo image (250/2; flip angle, 90°) demonstrates marked enhancement of the synovium (arrows), which is compatible with septic arthritis and diffuse enhancement of the distal tibia, indicating osteomyelitis. (c) Sagittal T1-weighted contrast-enhanced fat-suppressed fast multiplanar spoiled gradient-echo image (230/2; flip angle, 90°) demonstrates an ovoid lesion (arrow) in the distal tibia epiphysis with rim enhancement, which is compatible with a small intraepiphyseal abscess. (d) Coronal T1-weighted contrast-enhanced fat-suppressed fast multiplanar spoiled gradient-echo image (255/2; flip angle, 90°) demonstrates a small intraosseous sinus tract (arrow) that extends from the abscess to the articular surface of the tibia.

as the knee or hip, may not show signs of joint effusion in up to 16% of cases (14).

Hindfoot infection was present in one-fifth of the feet in which MR imaging was performed in our study, and ulcerations were seen predominantly over the heel

(15%). Reported frequencies of heel ulceration range from 6.3% to 26% in previous reports (24–26,36,37), which included mostly ambulatory patients. The relative frequency of heel ulceration in advanced infection is therefore compara-

ble with the prevalence in ambulatory patients. The most frequently infected bone in the hindfoot in our study was the calcaneus, and evidence of septic arthritis was seen in five ankle joints and two subtalar joints.

Several findings in our study are of direct importance to the radiologist. Most ulcers that require evaluation with MR imaging occur either at the proximal or distal end of the foot (in the heel and at the tip of the great toe) or at the lateral or medial border of the foot (at the fifth and first metatarsal heads). It is therefore important to image the entire volume of the forefoot or hindfoot, unless a targeted examination is performed in the region of the ulceration. Fat suppression may be incomplete at the forefoot because of inhomogeneity of the magnetic field or because the toes may extend out of the extremity coil. This may lead to diagnostic difficulties. Homogenous fat suppression can be assisted with plantar flexion of the foot or with the use of a standoff pad under the calcaneus. One-fourth of toe ulcers that require evaluation with MR imaging are located predominantly dorsally or medially over the interphalangeal joints in claw-toe deformities and may be less recognizable as ulcers at the plantar aspect.

Diagnosis of osteomyelitis with the use of MR imaging is based on identification of altered bone marrow signal intensity. Infection of the marrow compartment results in loss of normal fatty marrow signal intensity on T1-weighted images, with edema on T2-weighted or fast SE STIR images and enhancement on postcontrast gadolinium-enhanced T1-weighted images (38). Other entities, including fracture, tumors, severe inflammatory arthritis or neuropathic disease, and recent postoperative change, can alter the bone marrow signal intensity in a similar fashion (8,39–42). However, these entities can generally be distinguished from osteomyelitis on the basis of the pattern and location of the signal intensity abnormality, as well as associated findings in the adjacent bone, joint, or soft tissue (7). Review of our false-positive results revealed that osteomyelitis was often diagnosed in the presence of clearly visible signal intensity abnormalities that did not absorb contrast material on T1- and T2-weighted images. These signal intensity alterations represented either reactive hyperemic changes or subacute neuropathic osteoarthropathy thought to represent osteomyelitis, with little or no enhancement because of underlying vascular disease (11). Most false-negative results in our study could be attributed to

misinterpreting or overlooking subtle signal intensity changes, including small areas of enhancement. Another frequent cause of false-negative results was lack of enhancement due to severe vascular disease and established gangrene. No particular locations could be identified that led to erroneous diagnosis of osteomyelitis or lack thereof. No false-positive or false-negative results could be attributed to poor fat suppression, since we performed pre- and postcontrast fat-saturated fast multiplanar spoiled gradient-echo sequences in most patients. This technique allowed us to see contrast enhancement despite occasional heterogeneous fat suppression. In general, T2-weighted sequences, including fast SE STIR sequences, are more sensitive but less specific than T1-weighted and postcontrast sequences (7).

Definite diagnosis of osteomyelitis relies on culture of causative organisms from a biopsy sample (43). However, the accuracy of tissue evaluation in the diagnosis of osteomyelitis is, to our knowledge, unknown. Limitations of percutaneous and surgical bone biopsy include (44) sampling error, false-negative cultures in patients who receive antibiotics, difficulties in histopathologically distinguishing osteopathy from osteomyelitis, and risk of damaging the bone as a result of trauma or iatrogenic infection (34,45). Culture findings from percutaneous bone biopsy specimens obtained in patients with pedal infection may furthermore be unreliable because of contamination from underlying infected soft tissue (34,44,45). It has also been shown that bone biopsy cultures in patients with osteomyelitis may have false-negative results in up to 50% of cases (43), whereas accuracy of histopathologic diagnosis of osteomyelitis is high (46–49). White et al (43) therefore advocated both microbiologic and histologic evaluation of the bone samples to increase the sensitivity of the procedure.

Some limitations apply to our study. Our patient group was highly selected, since we wanted to study the distribution of pedal ulceration, osteomyelitis, and septic arthritis. It is probable that ulcerations were more obvious in this population than in a group selected at random, and, thus, may have led to a high sensitivity of diagnosis with the use of MR imaging. Sensitivity and specificity analysis of ulcer recognition on MR images would require a prospective study, since retrospective analysis of ulcer locations from patient reports does not provide reliable data to exclude ulceration. The selection of patients with advanced foot

infection may have also led to an overestimation of the specificity of MR imaging in the diagnosis of osteomyelitis. The presence of septic arthritis was confirmed in only a minority of patients by means of surgical reports. However, the diagnosis of septic arthritis in pedal infection may be specific, as discussed above.

We conclude that advanced pedal infection that is suggestive of osteomyelitis almost always results from contiguous infection and occurs predominantly in diabetic patients. Most ulcerations are seen in the forefoot, one-fifth are seen in the hindfoot, and ulcerations in the midfoot are rare. Ulcerations in the forefoot were most frequently seen in this selected population below the fifth and first metatarsal heads and at the tip of the great toe. In the hindfoot, most ulcers occurred in the heel. Pedal osteomyelitis and septic arthritis represent almost exclusively contiguous infections, occur most frequently around the fifth and first metatarsophalangeal joints, and mirror the distribution of pedal ulcers. Osseous spread of osteomyelitis is seen most frequently at the fifth and first metatarsophalangeal joints and spreads distally to the proximal phalanges. Evidence of septic arthritis is seen on MR images in one-third of patients suspected of having osteomyelitis.

References

1. Reiber GE, Lipsky BA, Gibbons GW. The burden of diabetic foot ulcers. *Am J Surg* 1998; 176(suppl 2A):S5–10S.
2. Boulton AJ, Vileikyte L. The diabetic foot: the scope of the problem. *J Fam Pract* 2000; 49(suppl 11):S3–S8.
3. Reiber GE, Boyko EJ, Smith G. Lower extremity foot ulcers and amputation in diabetes. In: Harris MI, ed. *Diabetes in America*. 2nd ed. Washington, DC: National Diabetes Data Group, 1995; 409–428.
4. Ramsey SD, Newton K, Blough D, et al. Incidence, outcomes, and cost of foot ulcers in patients with diabetes. *Diabetes Care* 1999; 22:382–387.
5. Wheat LJ, Allen SD, Henry M, et al. Diabetic foot infections: bacteriologic analysis. *Arch Intern Med* 1986; 146:1935–1940.
6. Bernhard LM, Bakst M, Coleman W, Nickamin A. Plantar space abscesses in the diabetic foot: diagnosis and treatment. *J Foot Surg* 1984; 23:283–290.
7. Morrison WB, Schweitzer ME, Batte WG, Radack DP, Russel KM. Osteomyelitis of the foot: relative importance of primary and secondary MR imaging signs. *Radiology* 1998; 207:625–632.
8. Beltran J, Campanini DS, Knight C, McCalla M. The diabetic foot: magnetic resonance imaging evaluation. *Skeletal Radiol* 1990; 19:37–41.
9. Marcus CD, Ladam-Marcus VJ, Leone J, Malgrange D, Bonnet-Gausserand FM, Menanteau BP. MR imaging of osteomy-

10. Beltran J. MR imaging of soft-tissue infection. *Magn Reson Imaging Clin N Am* 1995; 3:743–751.
11. Morrison WB, Schweitzer ME, Wapner KL, Hecht PJ, Gannon FH, Behm WR. Osteomyelitis in feet of diabetics: clinical accuracy, surgical utility, and cost-effectiveness of MR imaging. *Radiology* 1995; 196:557–564.
12. Craig JG, Amin MB, Wu K, et al. Osteomyelitis of the diabetic foot: MR imaging–pathologic correlation. *Radiology* 1997; 203:849–855.
13. Brower AC. Septic arthritis. *Radiol Clin North Am* 1996; 34:293–309.
14. Graif M, Schweitzer ME, Deely D, Matteucci T. The septic versus nonseptic inflamed joint: MRI characteristics. *Skeletal Radiol* 1999; 28:616–620.
15. Frykberg RG. Diabetic foot ulcers: current concepts. *J Foot Ankle Surg* 1998; 37:440–446.
16. Ctercteko GC, Dhanendran M, Hutton WC, Le Quesne LP. Vertical forces acting on the feet of diabetic patients with neuropathic ulceration. *Br J Surg* 1981; 68:608–614.
17. Veves A, Murray HJ, Young MJ, Boulton AJ. The risk of foot ulceration in diabetic patients with high foot pressure: a prospective study. *Diabetologia* 1992; 35:660–663.
18. Pham H, Armstrong DG, Harvey C, Harkless LB, Giurini JM, Veves A. Screening techniques to identify people at high risk for diabetic foot ulceration: a prospective multicenter trial. *Diabetes Care* 2000; 23:606–611.
19. Cavanagh PR, Ulbrecht JS, Caputo GM. Biomechanical aspects of diabetic foot disease: aetiology, treatment, and prevention. *Diabet Med* 1996; 13(suppl 1):S17–S22.
20. Stadelmann WK, Digenis AG, Tobin GR. Impediments to wound healing. *Am J Surg* 1998; 176(suppl 2A):39S–47S.
21. Gibbons GW, Habershaw GM. Diabetic foot infections: anatomy and surgery. *Infect Dis Clin North Am* 1995; 9:131–142.
22. Birke JA, Franks BD, Foto JG. First ray joint limitation, pressure, and ulceration of the first metatarsal head in diabetes mellitus. *Foot Ankle Int* 1995; 16:277–284.
23. Hill SL, Holtzman GI, Buse R. The effects of peripheral vascular disease with osteomyelitis in the diabetic foot. *Am J Surg* 1999; 177:282–286.
24. Walters DP, Gatling W, Mullee MA, Hill RD. The distribution and severity of diabetic foot disease: a community study with comparison to a non-diabetic group. *Diabet Med* 1992; 9:354–358.
25. Jones EW, Peacock I, McLain S, et al. A clinico-pathological study of diabetic foot ulcers. *Diabet Med* 1987; 4:475–479.
26. Isakov E, Budoragin N, Shenhav S, Mendelovich I, Korzets A, Susak Z. Anatomic sites of foot lesions resulting in amputation among diabetics and non-diabetics. *Am J Phys Med Rehabil* 1995; 74:130–133.
27. Apelqvist J, Castenfors J, Larsson J, Stenstrom A, Agardh CD. Wound classification is more important than site of ulcer-

- ation in the outcome of diabetic foot ulcers. *Diabet Med* 1989; 6:526–530.
28. Boulton AJ, Hardisty CA, Betts RP, et al. Dynamic foot pressure and other studies as diagnostic and management aids in diabetic neuropathy. *Diabetes Care* 1983; 6:26–33.
 29. Mueller MJ, Minor SD, Diamond JE, Blair VP III. Relationship of foot deformity to ulcer location in patients with diabetes mellitus. *Phys Ther* 1990; 70:356–362.
 30. Gibbs RC, Boxer MC. Abnormal biomechanics of feet and their cause of hyperkeratoses. *J Am Acad Dermatol* 1982; 6:1061–1069.
 31. Levin ME. Foot lesions in patients with diabetes mellitus. *Endocrinol Metab Clin North Am* 1996; 25:447–462.
 32. Lavery LA, Lavery DC, Quebedeaux-Farnham TL. Increased foot pressures after great toe amputation in diabetes. *Diabetes Care* 1995; 18:1460–1462.
 33. Garbalosa JC, Cavanagh PR, Wu G, et al. Foot function in diabetic patients after partial amputation. *Foot Ankle Int* 1996; 17:43–48.
 34. Bamberger DM, Daus GP, Gerding DN. Osteomyelitis in the feet of diabetic patients: long-term results, prognostic factors, and the role of antimicrobial and surgical therapy. *Am J Med* 1987; 83:653–660.
 35. Weishaupt D, Schweitzer ME, Alam F, Karasick D, Wapner K. MR imaging of inflammatory joint diseases of the foot and ankle. *Skeletal Radiol* 1999; 28:663–669.
 36. Kaufman J, Breeding L, Rosenberg N. Anatomic location of acute diabetic foot infection: its influence on the outcome of treatment. *Am Surg* 1987; 53:109–112.
 37. Lithner F, Tornblom N. Gangrene localized to the feet in diabetic patients. *Acta Med Scand* 1984; 215:75–79.
 38. Morrison WB, Schweitzer ME, Bock GW, et al. Diagnosis of osteomyelitis: utility of fat-suppressed contrast-enhanced MR imaging. *Radiology* 1993; 189:251–257.
 39. Daffner RH, Lupetin AR, Dash N, Deeb ZL, Sefczek RJ, Schapiro RL. MRI in the detection of malignant infiltration of bone marrow. *AJR Am J Roentgenol* 1986; 146:353–358.
 40. Gold RH, Tong DJ, Crim JR, Seeger LL. Imaging the diabetic foot. *Skeletal Radiol* 1995; 24:563–571.
 41. Jelinek J, Pearl AB, Kominsky SJ, Schultz PM. Magnetic resonance imaging of the foot: rheumatologic disorders mimicking osteomyelitis. *J Am Podiatr Med Assoc* 1996; 86:228–231.
 42. Seabold JE, Flickinger FW, Kao SC, et al. Indium-111-leukocyte/technetium-99m-MDP bone and magnetic resonance imaging: difficulty of diagnosing osteomyelitis in patients with neuropathic osteoarthropathy. *J Nucl Med* 1990; 31:549–556.
 43. White LM, Schweitzer ME, Deely DM, Gannon F. Study of osteomyelitis: utility of combined histologic and microbiologic evaluation of percutaneous biopsy samples. *Radiology* 1995; 197:840–842.
 44. Lipsky BA, Pecoraro RE, Wheat LJ. The diabetic foot: soft tissue and bone infection. *Infect Dis Clin North Am* 1990; 4:409–432.
 45. Wheat J. Diagnostic strategies in osteomyelitis. *Am J Med* 1985; 78:218–224.
 46. Carrasco CH, Wallace S, Richli WR. Percutaneous skeletal biopsy. *Cardiovasc Intervent Radiol* 1991; 14:69–72.
 47. Mushlin AI, Littenberg B. Diagnosing pedal osteomyelitis: testing choices and their consequences. *J Gen Intern Med* 1994; 9:1–7.
 48. Howard CB, Einhorn M, Dagan R, Yagupski P, Porat S. Fine-needle bone biopsy to diagnose osteomyelitis. *J Bone Joint Surg Br* 1994; 76:311–314.
 49. Sugarman B, Hawes S, Musher DM, Klima M, Young EJ, Pircher F. Osteomyelitis beneath pressure sores. *Arch Intern Med* 1983; 143:683–688.